Absence of Nogo-B (Reticulon 4B) facilitates hepatic stellate cell apoptosis and diminishes hepatic fibrosis in mice

Keitaro Tashiro[1], Ayano Satoh[2], Teruo Utsumi[1], Chuhan Chung[1] and Yasuko Iwakiri[1,*]

1. Section of Digestive Diseases, Department of Internal Medicine, Yale University School of Medicine, New Haven, CT, U.S.A.
2. Graduate School of Natural Sciences, Okayama University, Okayama, Japan

Short running head: Nogo-B, hepatic apoptosis and fibrosis

*** Corresponding author: Yasuko Iwakiri, Ph.D.**

1080 LMP, 333 Cedar Street, Section of Digestive Diseases,

Yale University School of Medicine, New Haven, CT 06520

U.S.A.

e-mail: yasuko.iwakiri@yale.edu

Phone #: 203-785-6204

Fax #: 203-785-7273

Grant support: This work was supported by grants R01DK082600 and Yale Liver Center Pilot Project Award (P30-34989) from the National Institutes of Health (Iwakiri), Female Researcher Science Grant from Shiseido Japan (Satoh) and VA merit award (Chung).

Number of text pages: 27
Figures: 7
Keywords: apoptosis, ER stress, myofibroblasts
Body text: 3,998 words – including figure legends and references

Abstract

Background Nogo-B (Reticulon 4B) accentuates hepatic fibrosis and cirrhosis, but the mechanism remains unclear. The aim of this study was to identify Nogo-B's role in hepatic stellate cell (HSC) apoptosis in cirrhotic livers.

Methods Cirrhosis was generated by carbon tetrachloride inhalation in wild-type (WT) and Nogo-A/B knockout (NGB KO) mice. HSCs were isolated from WT and NGB KO mice and cultured for activation and transformation to myofibroblasts (MF-HSCs). Human hepatic stellate cells (LX2) were used to assess apoptotic responses of activated HSCs after silencing or overexpressing NGB.

Results Livers from cirrhotic NGB KO mice demonstrated significantly reduced fibrosis ($p = 0.012$) compared with those of WT mice. Apoptotic cells were more prominent in fibrotic areas of cirrhotic NGB KO livers. NGB KO MF-HSCs revealed significantly elevated levels of apoptotic markers, cleaved PARP, caspase-3 and -8 ($p < 0.05$), compared with WT MF-HSCs in response to staurosporine (STS). Treatment with tunicamycin, an ER stress inducer, increased cleaved caspase-3 and -8 levels in NGB KO MF-HSCs compared with WT MF-HSCs ($p < 0.01$). In LX2 cells, NGB knockdown enhanced apoptosis in response to STS, whereas NGB overexpression inhibited apoptosis.

Conclusion The absence of Nogo-B enhances apoptosis of HSC in experimental cirrhosis. Selective blockade of Nogo-B in HSCs may represent a potential therapeutic strategy to mitigate liver fibrosis.

215 words (220 words limit)

Introduction

Liver fibrosis and its end-stage manifestation cirrhosis represent clinical challenges worldwide. Hepatic stellate cell (HSC) activation is the cardinal feature that results in hepatic fibrosis. When stimulated by reactive oxygen species or cytokines in response to various hepatic insults, quiescent HSCs are transformed to myofibroblasts (MF-HSCs) that proliferate and secrete collagen.[1-4] Studies have demonstrated that apoptosis of activated HSCs can reverse fibrosis.[5-13] Thus, the mechanisms that control MF-HSC apoptosis may represent potential therapeutic targets that result in fibrosis resolution.[14-16]

Nogo-B, also known as Reticulon 4B, is a member of the reticulon protein family that are localized primarily to the endoplasmic reticulum (ER).[17, 18] Four groups of Reticulons, 1, 2, 3 and 4, exist with each having multiple isoforms. Reticulon 4 has three isoforms, Nogo-A, B and C. The most recognized isoform, Nogo-A (200 kDa), a potent neural outgrowth inhibitor,[19-21] is mainly expressed in the nervous system.[22-24] Nogo-C (25 kDa) is highly expressed in the differentiated muscle fibers and somewhat in the brain;[17, 18, 22] its function remains unclear.

Nogo-B (55 kDa), a splice variant of Nogo-A, is expressed in most tissues and has been reported for its role in modulating endothelial and smooth muscle cellular responses following injury in a variety of organs/tissues, including blood vessels,[25, 26] lung,[27, 28] kidney,[29] and liver.[30] We previously demonstrated that the absence of Nogo-B in a murine model blocks the progression of fibrosis/cirrhosis and the development of portal hypertension.[30] Further, we showed that lack of Nogo-B decreases the levels of α-smooth muscle actin (α-SMA), a marker of MF-HSCs, in murine cholestatic livers. These findings led us to hypothesize that absence of Nogo-B may increase the susceptibility of MF-HSCs to apoptosis thereby reducing fibrosis/cirrhosis in mice. In this study, we investigated the role of Nogo-B in MF-HSC apoptosis *in vivo* and *in vitro*.

Materials and Methods

Animals

All animal studies were approved by the Institutional Animal Care and Use Committees of Yale University and Veterans Affairs Connecticut Healthcare System. Studies were performed in adherence with the National Institutes of Health Guide for the Care and Use of Laboratory Animals. Nogo-A/B knockout (NGB KO) mice were a gift from Stephen Strittmatter[31] and Mark Tessier-Lavigne.[32]

Induction of hepatic fibrosis and cirrhosis

Five male NGB KO and their littermate wild-type (WT) mice at the age of 1 month were exposed to carbon tetrachloride (CCl_4) by inhalation for 12 weeks.[33, 34] Phenobarbital (0.35 g/L) was added to the drinking water 3 days prior to CCl_4 exposure to accentuate fibrosis/cirrhosis. Mice were placed in a gas chamber (60 x 40 x 20 cm) under a fume hood and exposed to CCl_4 gas three times a week. The duration of CCl_4 inhalation was 1–2 minutes for the first 3 weeks and was increased to 3–5 minutes thereafter. CCl_4 exposure was stopped 5–7 days before the experiment. Phenobarbital was no longer added to the drinking water at the time CCl_4 exposure was stopped. Age-matched untreated WT and NGB KO mice were used as treatment controls. Liver samples were isolated and fixed in formalin. Paraffin-embedded liver samples were prepared for histological analyses.

Sirius red staining

Histological specimens were embedded in paraffin and cut to 6μm-thick sections. Sections were deparaffinized by three-time washes of xylene for 5 minutes each, and rehydrated with 100%, 90% and 70% ethanol for 5minutes each. After rinsing in distilled water for 5 minutes, sections were incubated in 0.1% Sirius

red solution (Sigma-Aldrich, St. Louis, MO) for 90 minutes, soaked in 0.5% acetic acid buffer, and dehydrated gradually with 70%, 90% and 100% ethanol and 3 times with xylene for 5 minutes. Fibrosis was determined by calculating the percent Sirius red–positive area (i.e., collagen-positive area) over the total area analyzed. Image J1.43u (Wayne Rasband, National Institutes of Health, Bethesda, MD) was used for image analysis of the entire liver sections. At least 20 images per liver section were randomly taken and used for the analyses.[30]

Immunohistochemistry

Paraffin-embedded sections (6μm-thick) were deparaffinized and rehydrated as described above. Antigen retrieval was performed by placing sections in 10mM sodium citrate buffer pH 6.0, heated in a microwave, placed in a steamer for 30 minutes, and steadily cooled down on the bench top for 20 minutes. Sections were then treated with 3% hydrogen peroxidase diluted with methanol, followed by blocking with 5% Donkey serum plus 1% bovine serum albumin (BSA) in PBS. After blocking non-specific biotin and avidin using a kit (Avidin/Biotin blocking kit, Vector Laboratories, Burlingame, CA), sections were incubated overnight at 4^{o}C with cleaved caspase-3 antibody (rabbit, 1:100, Cell Signaling, Danvers, MA). After washing three times with Tris-buffered saline with 0.05% Tween20 (TBST) for 5 minutes, sections were incubated with biotinylated anti-rabbit IgG (1:500, Jackson ImmunoResearch Laboratories, West Grove, PA) and avidin conjugated horse radish peroxidase (Vector Laboratories) for 30 minutes each at room temperature. After washing three times with TBST, sections were incubated with DAB substrate (Vector Laboratories) for color development, followed by counterstaining with hematoxylin. Sections were then dehydrated and mounted. Images were taken using a light microscope (Eclipse 80i, Nikon, Melville, NY) and analyzed by Image J1.43u.

Dual staining of TdT-mediated dUTP nick-end labeling (TUNEL) and α-SMA

O.C.T.-embedded frozen liver tissues were cut to 6μm-thick sections and fixed with 4% paraformaldehyde (PFA) in PBS for 20 minutes at room temperature, followed by washing with PBS three times for 5 minutes each. Antigen retrieval was performed by placing sections in 10mM sodium citrate buffer pH 6.0, heated in a microwave, placed in a steamer for 30 minutes, and steadily cooled down on the bench top for 20 minutes. Sections were then incubated with a blocking buffer including 5% Donkey serum plus 1% BSA in PBS-0.3% Triton-X for 1 hour, followed by the treatment with mouse Ig blocking reagent (Vector Laboratories) for 1 hour at room temperature. Sections were then incubated with a mouse monoclonal anti-αSMA (1:1,000; Sigma-Aldrich) at room temperature for 1 hour. After washing three times with TBST for 5 minutes each, sections were incubated with Alexa Fluor 555 donkey anti-mouse IgG (1:500; Invitrogen, Grand Island, NY) for 30 minutes at room temperature. After these processes, TUNEL staining was performed using a commercial kit (*In Situ* Cell Death Detection Kit; Roche Diagnostics, Indianapolis, IN) for 1 hour at room temperature. After washing three times with TBST for 5 minutes each, sections were mounted with a DAPI containing media (Invitrogen). Images were taken by a fluorescent microscope (Eclipse E800; Nikon) and recorded using Openlab3 software (PerkinElmer, Waltham, MA).

Isolation of hepatic stellate cells (HSCs)

Primary HSCs were isolated from WT and NGB KO mice by in situ perfusion of livers with pronase-collagenase, followed by density gradient centrifugation using Nycodenz (Histodenz; Sigma-Aldrich) density gradients as described.[35, 36] HSCs were cultured in Dulbecco's Modified Eagle's Medium with high glucose (DMEM; GIBCO, Invitrogen) supplemented with 10% fetal bovine serum (FBS), antibiotics (100 U/mL penicillin and 100 μg/mL streptomycin) and 1% L-glutamine in humidified air containing 5% CO_2 at 37^{o}C. HSCs were cultured for more than 14 days to fully transform to myofibroblasts (MF-HSCs).[37]

Treatment of MF-HSCs with staurosporine, FAS ligand and tunicamycin

MF-HSCs were seeded in 6-well tissue culture plates at a density of 2.0 x 10^5 cells/well and incubated in humidified air containing 5% CO_2 at 37^{o}C overnight. Media was changed to serum free conditions in DMEM for 24 hours, and MF-HSCs were treated with 1μM staurosporine (STS; Calbiochem, Germany) for 0, 2, 4, 6, 8 and 10 hours to induce apoptosis. To determine whether apoptosis was Fas receptor dependent, MF-HSCs were treated with 50 ng/mL Fas ligand (FasL; Calbiochem) in the presence of 20 ng/mL cycloheximide (CHX; Calbiochem) for 10 hours. To induce ER stress, MF-HSCs were treated with tunicamycin at concentrations of 0, 0.5, 1, 2, 5 and 10 μM for 24 hours.

Hepatocyte isolation

Hepatocytes were isolated from WT and Nogo-B KO mice by collagenase perfusion as previously described[38] with slight modifications. Briefly, cells were cultured on collagen-coated cell culture dishes or glass coverslips in Hepatocyte Maintenance Medium (HMM; Clonetics/Lonza, Basel, Switzerland) supplemented with HMM SingleQuots (Clonetics/Lonza) and Matrigel (BD Biosciences, San Jose, CA). An initial coating density was 0.4x10^6/ml. On the following day, cells were replaced with medium without any supplementation and incubated for 24 hours. Cells were then subjected to experiments for STS treatment.

Western blot analysis

After drug treatment, cells were collected in a lysis buffer containing 50mM Tris HCl, 0.1mM EGTA, 0.1mM EDTA, 0.1% SDS, 0.1% deoxycholic acid, 1% (vol/vol) Nonidet P-40, 5mM sodium fluoride, 1mM sodium pyrophosphate, 1mM activated sodium vanadate, 0.32% protease inhibitor cocktail (Roche Diagnostics),

and 0.027% Pefabloc (Roche Diagnostics). Lysates were centrifuged at 14,000 rpm, 4°C for 10 minutes. Protein concentration was determined using a Lowry assay. An equal amount of protein (10-20 μg) from each sample was loaded onto sodium dodecyl sulfate-polyacrylamide gel electrophoresis (SDS-PAGE) gels and transferred to 0.2 μm nitrocellulose membranes (BIO-RAD, Hercules, CA). After blocking with 5% nonfat dry milk in 0.1% TBST, membranes were probed with rabbit anti-Nogo serum (1761A, 1:10,000, a kind gift from Dr. William C. Sessa, Yale University), goat anti-Nogo (N-18, 1:200; Santa Cruz Biotechnology Inc., Santa Cruz, CA), mouse anti-Hsp90 (1:1000; BD Biosciences), mouse anti-Bip (1:1000; BD Biosciences), rabbit anti-PARP (1:1,000; Cell Signaling), rabbit anti-cleaved caspase-3 (1:1,000; Cell Signaling), rabbit anti-cleaved caspase-8 (1:1,000; Cell Signaling), rabbit anti-Bcl-xL (1:1,000; Cell Signaling), mouse anti-caspase-9 (1:1,000; Cell Signaling), or mouse anti-β actin (1:5,000; Sigma-Aldrich). After washing three times with TBST for 10 minutes, membranes were incubated with fluorophore-conjugated secondary antibodies (either 680nm or 800nm emission). Detection and quantification of bands were performed using the Odyssey Infrared Imaging System (Li-Cor Biotechnology, Lincoln, NE). Hsp90 and β-actin were used for loading controls.

TUNEL and Annexin V staining

MF-HSCs were fixed with 4% paraformaldehyde (PFA) in PBS for 1 hour at room temperature, followed by washing with PBS three times for 5 minutes each. MF-HSCs were then incubated with a permeabilization buffer containing 0.1% Triton X-100 in 0.1% sodium citrate on ice for 5 minutes. TUNEL staining was performed using a commercial kit (*In Situ* Cell Death Detection Kit; Roche Diagnostics) by incubating MF-HSCs for 1 hour at room temperature. Recombinant DNase I (Roche Diagnostics) 3 U/mL was incubated for 10 minutes as a positive control prior to labeling procedures. The label solution conjugated with fluorescein alone was used as a negative control. After washing three times with PBS for 5 minutes each,

MF-HSCs were mounted with a mounting media containing DAPI (Invitrogen). Annexin V staining was performed using Alexa Fluor 488-conjugated Annexin V/Dead Cell Apoptosis Kit (Molecular Probes; Invitrogen). Images were taken using a fluorescent microscope (Eclipse E800; Nikon) and recorded with Openlab3 software (PerkinElmer).

Nogo-B knockdown in human hepatic stellate cell line (LX2)

LX-2 cells were a kind gift from Dr. Scott L. Friedman (Mount Sinai School of Medicine, NY).[39] Cells were seeded in 6-well tissue culture plates at a density of 1.5 x 10^5 cells/well and incubated in humidified air containing 5% CO_2 at 37°C for overnight. Cells were transfected with 100nM Nogo-B siRNA in 750 μL OptiMEM (GIBCO, Invitrogen) with 2 μl Oligofectamine (Invitrogen) and incubated for 6 hours. Then, 750 μL of DMEM containing 20% FBS and 2% L-glutamine was added to each well. After 48 hours of incubation, these cells were starved in DMEM without FBS for 24 hours and treated with 100nM STS for0, 2, 4, 6, 8, and 10 hours.

Nogo-B overexpression in LX2

LX2 cells were seeded in 12-well tissue culture plates at a density of 1.0 x 10^5 cells/well and incubated in humidified air containing 5% CO_2 at 37°C for overnight. Cells were transfected with 0.5 μg of HA-tagged Nogo-B plasmid (or pcDNA3 vector alone as a negative control) in 500 μL OptiMEM (GIBCO, Invitrogen) with 1.5 μl FuGENE 6 (Roche Diagnostics) and incubated for 6 hours. Then, 500 μL of DMEM containing 10% FBS and 1% L-glutamine was added to each well. After 48 hours of incubation, cells were starved in DMEM without FBS for 24 hours, followed by the treatment with 100nM STS for 4 and 8 hours.

For immunocytochemistry, cells were washed with cold PBS and fixed with 4% PFA in PBS for 20 minutes at room temperature. After washing three times with PBS for 5 minutes each, cells were incubated in a

buffer containing 0.3% Triton X-100, 5% donkey serum and 1% BSA in PBS at room temperature for 1 hour. After washing with PBS, cells were incubated with antibodies including rat anti-HA (1:1,000; Roche Diagnostics) and rabbit anti-cleaved caspase-3 (1:1,000; Cell Signaling), which were diluted with 1% BSA in PBS at 4^{o}C for overnight. Cells were then incubated with Alexa Fluor 488 donkey anti-rat IgG (1:500; Invitrogen) or Alexa Fluor 588 donkey anti-Rabbit IgG (1:500; Invitrogen) as a secondary antibody for 1 hour at room temperature. Cells were mounted with a DAPI containing media (Invitrogen). Images were taken by a fluorescent microscope (Eclipse E800; Nikon) and recorded using Openlab3 software (PerkinElmer).

Statistical analysis

Data were expressed as mean $\pm$ standard error (SE). Statistical differences among the mean values of multiple groups were determined using analysis of variance (ANOVA) followed by a Student *t* test. Values of $p < 0.05$ were considered statistically significant.

Results

Lack of Nogo-B reduces fibrosis and facilitates apoptosis in fibrotic areas of the mouse cirrhotic liver.

Sirius red staining was performed in cirrhotic livers isolated from WT and NGB KO mice that underwent CCl_4 inhalation for 12 weeks (Figure 1A left panel). Liver fibrosis was significantly reduced in NGB KO livers compared with WT livers (Figure 1A left and right panels, $p = 0.012$). This is similar to the results observed using a murine model of bile duct ligation (BDL).[30] Apoptotic cells, as indicated by cleaved caspase-3 immunolabeling, were seen in fibrotic regions of Nogo-B KO livers, whereas they were much less apparent in WT livers (Figure 1B). NGB KO cirrhotic livers demonstrated co-localization of TUNEL staining with α-SMA positive cells, while TUNEL staining was not apparent in WT cirrhotic livers (Figure 1C). These results suggest that the lack of Nogo-B reduces fibrosis and enhances apoptosis of activated HSCs in experimental cirrhosis.

Lack of Nogo-B facilitates apoptosis of myofibroblasts derived from hepatic stellate cells (MF-HSCs).

Nogo-B's role in apoptosis of MF-HSCs was examined using staurosporine (STS), an inducer of apoptosis.[40-42] WT and NGB KO MF-HSCs were treated with 1μM STS for 16 hours and examined for TUNEL and Annexin V labeling. NGB KO MF-HSCs showed significantly higher percentages of TUNEL and Annexin V positive nuclei compared with WT MF-HSCs (Figures 2A and B, $p < 0.01$).

We also determined the levels of several apoptotic markers in WT and NGB KO MF-HSCs after treatment with 1μM STS for 0, 2, 4, 6, 8 and 10 hours (Figure 3). Levels of cleaved PARP were increased in a time-dependent manner in both WT and NGB KO MF-HSCs, but were significantly higher in NGB KO MF-HSCs 4, 6 and 10 hours after STS treatment ($p < 0.05$ for 4 and 6 hours and $p < 0.01$ for 10 hours, Figure 3B top panel). Similarly, cleaved caspase-3 levels were significantly increased in NGB KO MF-HSCs 4, 6 and 8 hours after STS

treatment ($p < 0.05$ for 4 and 6 hours and $p < 0.01$ for 8 hours, Figure 3B middle panel). The levels of cleaved caspase-8 were also significantly increased in NGB KO MF-HSC 4, 6 and 8 hours after STS treatment ($p < 0.05$, Figure 3B bottom left panel). Cleaved caspase-9 and Bcl-xL levels did not differ between these two groups at all time points examined (Figure 3B bottom middle and right panels). This may reflect the fact that Bcl-xL primarily acts on mitochondria and prevents apoptosis by inhibiting the activity of caspase-9.[43, 44] These results indicate that the lack of Nogo-B facilitates apoptosis of MF-HSCs in response to STS.

Lack of Nogo-B does not influence hepatocyte apoptosis in response to staurosporine (STS).

To investigate the possibility that Nogo-B may modulate apoptosis in hepatocytes, hepatocytes from WT and NGB KO mice were treated with STS (Figure 4). Hepatocytes required a higher dose of STS than MF-HSCs to induce apoptosis (10 vs. 1 μM, respectively). Moreover, there was no difference in the levels of apoptotic markers between WT and NGB KO hepatocytes. These results indicate that the absence of NGB preferentially sensitize MF-HSCs rather than hepatocytes to apoptosis under conditions of experimental cirrhosis.

Knockdown of Nogo-B increases apoptosis in human hepatic stellate cells (LX2).

To confirm Nogo-B's role in apoptosis in human MF-HSCs, LX2 cells were transfected with Nogo-B siRNA to suppress Nogo-B expression. We then tested apoptosis in those cells, treated with100nM STS for 0, 2, 4, 6, 8 and 10 hours (Figure 5). Nogo-B siRNA resulted in 66% reduction of Nogo-B expression. Similar to the results in mouse MF-HSCs, the levels of cleaved PARP and caspase-3 were increased in LX2 cells treated with NGB siRNA compared with controls, while the levels of cleaved caspase-9 and Bcl-xL did not differ. Consistent with mouse MF-HSCs, knockdown of Nogo-B resulted in enhanced apoptosis in human MF-HSCs in response to STS.

Overexpression of Nogo-B blocks apoptosis in human hepatic stellate cells (LX2).

To determine the effect of Nogo-B overexpression on apoptosis of human MF-HSCs, LX2 cells were transfected with HA-tagged human Nogo-B plasmid and treated with 100nM STS for 8 hours. The transfection resulted in a 7-fold higher level of Nogo-B over the endogenous Nogo-B level found in non-transfected LX-2 cells (data not shown). As shown in Figure 6, the majority of HA-Nogo-B positive cells (green staining) were negative for cleaved caspase-3 (red staining). In fact, the percentage of cleaved caspase-3 positive cells was significantly lower in HA-Nogo-B positive cells than in non-transfected cells (4.2 vs. 29.4%, respectively, $p < 0.01$). These results suggest that MF-HSCs become resistant to apoptosis with Nogo-B overexpression. This data also lends support to our earlier data that the lack of Nogo-B facilitates apoptosis of MF-HSCs.

Nogo-B is involved in ER stress-induced apoptosis in myofibroblasts derived from hepatic stellate cells (MF-HSCs).

In order to examine how Nogo-B influences apoptosis of MF-HSCs, WT and NGB KO MF-HSCs were treated with tunicamycin, an ER stress inducer, and Fas ligand (FasL), an inducer of apoptosis through the death receptor pathway. Tunicamycin treatment (0, 0.5, 1, 2, 5 and 10 μg/mL for 24 hours) generated significantly higher levels ($p < 0.01$) of cleaved caspase-3 and -8 in NGB KO MF-HSCs than in WT MF-HSCs virtually at all concentrations examined, while the levels of Bip, a marker of the ER stress response, were similar in WT and NGB KO MF-HSCs (Figure 7A upper panels). In contrast, FasL treatment (50 ng/mL for 10 hours in the presence of 20 ng/mL cycloheximide) did not affect the levels of apoptotic markers (cleaved PARP, cleaved caspase-3 and -8) between WT and NGB KO MF-HSCs (Figure 7B). In addition, levels of Bcl-xL, which is related to the mitochondrial pathway of apoptosis, was not different between WT and NGB KO MF-HSCs in

response to STS (Figure 3B bottom left panel). These results suggest that the higher degree of apoptosis observed in NGB KO MF-HSCs is attributable in part to ER stress-induced apoptosis (Figure 7C).

Discussion

Experimental studies have demonstrated that inducing HSC apoptosis may reverse hepatic fibrosis.[45-49] In this study, we have discovered that lack of Nogo-B reduces liver fibrosis and enhances apoptosis of myofibroblasts derived from HSCs (MF-HSCs, i.e., activated HSCs) in mice that underwent carbon tetrachloride (CCl_4) inhalation for 12 weeks. Enhanced apoptosis due to the absence of Nogo-B was recapitulated *in vitro* as well. Cultured myofibroblasts derived from HSCs of Nogo-B KO mice as well as human hepatic stellate cells (LX2) with Nogo-B gene knockdown demonstrated a greater degree of apoptosis than their respective controls in response to an apoptotic stimulus. Furthermore, Nogo-B overexpression decreased susceptibility of LX2 cells to apoptosis. These findings suggest that Nogo-B has an anti-apoptotic effect on MF-HSCs and that the enhanced apoptosis of MF-HSCs lacking Nogo-B may be responsible for the reduced fibrosis observed in the livers of Nogo-B KO mice.

We previously reported that Nogo-B levels are elevated in fibrotic areas of human cirrhotic liver specimens as well as in mouse cholestatic models of fibrosis after bile duct ligation. Nogo-B gene deletion blocks the progression of liver cirrhosis and portal hypertension, suggesting that Nogo-B promotes liver fibrosis. This anti-fibrotic effect was mediated through TGFβ/Smad2 signaling in myofibroblasts.[30] The current study adds to these earlier findings by showing that Nogo-B represents an anti-apoptotic factor for HSCs in the setting of experimental cirrhosis. Moreover, this study confirms that Nogo-B facilitates fibrosis in the CCl_4 model of cirrhosis and supports our earlier studies that demonstrate a pro-fibrotic role for Nogo-B in the liver. Previous work using Nogo-B KO mice in a kidney injury model observed no significant differences in tissue fibrosis.[29] The length of injury and the different organ systems studied may account for these different outcomes.

We have also examined pathways through which Nogo-B carries out anti-apoptosis of MF-HSCs with a

focus on ER stress, Fas ligand, and mitochondrial pathways. Since ER stress induces apoptosis in HSCs[12] and Nogo-B regulates ER structure,[17, 18, 28, 50] we hypothesized that Nogo-B's anti-apoptotic effect on MF-HSCs might be mediated by ER stress. In fact, treatment with tunicamycin significantly increased the levels of cleaved caspase-3 and -8 in Nogo-B KO MF-HSCs, compared with their WT counterparts. These indicate that Nogo-B's anti-apoptotic role in MF-HSCs is due, at least in part, to its involvement in ER stress (Figure 7C). Thus, Nogo-B appears to increase the susceptibility of MF-HSCs to ER stress thereby predisposing to apoptosis.

In contrast, our study indicates that Nogo-B's anti-apoptotic role in MF-HSCs is not likely via the mitochondrial pathway, since the level of Bcl-xL, an indicator of mitochondria-mediated apoptosis, did not differ between WT and Nogo-B KO MF-HSCs in response to staurosporine. Although we found significantly higher levels of cleaved caspase-8 in Nogo-B KO MF-HSCs in response to staurosporine, caspase-8 is known to be activated through the ER stress pathway[51] and/or the death receptor pathway.[52-54] In addition, treatment with FasL, a pro-apoptotic death ligand, did not generate any difference in the level of cleaved caspase-8 between these two groups of MF-HSCs ruling out a role for Fas mediated cell death.

Nogo-B's involvement in apoptosis has also been reported in cancer cells. However, those reports are conflicting. One study shows increased apoptosis in HeLa derived D98/AH2 cells transiently transfected with Nogo-B.[55] Another study also presents Nogo-B's pro-apoptotic effect on CGL4 (a HeLa-derived cell line), SaOS-2 (an osteosarcoma cell line), MeWo (a melanoma cell line), HT-1080 (a fibrosarcoma cell line) and HFL (the immortalized, non-malignant, human fibroblast cell line), having them transiently transfected with Nogo-B.[56] In contrast, Oertle et al. document that SaOS-2 stably transfected with Nogo-B does not differ in the apoptotic effect from its control.[57] These discrepancies may suggest that timing and length of Nogo-B overexpression are a key to induce apoptosis in certain cancer cells and that those cancer cells with stable overexpression of Nogo-B might develop an adaptive machinery that protects them from apoptosis. Further studies are needed to clarify

these contradictions. An anti-apoptotic role of Nogo-B has also been observed in lung cells in pulmonary hypertension.[28] Overall, Nogo-B may function as a pro-apoptotic or anti-apoptotic protein, depending on the specific cell type.

Apoptosis can also mediate pro-fibrotic responses in the liver depending on the cell type involved. Hepatocyte apoptosis is thought to facilitate fibrosis by triggering and maintaining HSC activation in response to hepatic insults.[58] To address this issue, we examined whether the levels of apoptotic markers (cleaved PARP, cleaved caspase-3 and-8, and Bcl-xL) in cultured WT and Nogo-B KO hepatocytes differed in response to staurosporine. No differences in apoptotic activity were observed, indicating that Nogo-B's anti-apoptotic effect is specific to MF-HSCs.

In conclusion, absence of Nogo-B specifically increases apoptotic responses of MF-HSCs, which is associated with a reduction in hepatic fibrosis. Therefore, Nogo-B may be a potential target for the treatment of liver fibrosis/cirrhosis.

Acknowledgements

We would like to thank Ms. Kathy M. Harry for hepatocyte isolation (Yale Liver Center Cell Isolation Core Facility).

Figure Legends

Figure 1

Lack of Nogo-B decreases liver fibrosis and increases apoptotic cells in fibrotic areas in mice.

A. Representative images of Sirius red staining (left panel, Scale bar; 100μm) and percentages of Sirius red positive areas in cirrhotic livers from wild-type (WT) and NGB KO mice. Values represent mean ± standard error (SE) (* $p < 0.05$). **B.** Immunohistochemistry of cleaved caspase-3 in cirrhotic livers isolated from WT and NGB KO mice (Scale bar; 100μm). Red arrowheads in the enlarged images (lower panel) indicate cleaved caspase-3 positive cells in the fibrotic area. Serial liver sections from the same mice were stained for Sirius red and cleaved caspase-3. At least 5 images were taken for each group. **C.** Co-localization of apoptotic cells with alpha-smooth muscle actin (α-SMA) in cirrhotic livers isolated from WT and NGB KO mice that underwent bile duct ligation (Scale bar; 50μm). α-SMA is shown in red, apoptotic (TUNEL positive) cells in green, and nuclei stained with DAPI in blue. Arrowheads indicate apoptotic cells. At least 5 images were taken for each group.

Figure 2

Lack of Nogo-B facilitates apoptosis of mouse myofibroblasts derived from hepatic stellate cells (MF-HSCs) *in vitro*.

MF-HSCs were treated with 1μM staurosporine (STS) for 16 hours to induce apoptosis. **A.** TUNEL staining (green: TUNEL positive nuclei, blue: DAPI, Scale bar; 100μm) and percentages of TUNEL positive nuclei in WT and NGB KO MF-HSCs. **B.** Annexin V staining (green: Annexin V positive nuclei, blue: DAPI, Scale bar; 100μm) and percentages of Annexin V positive nuclei in WT and NGB KO MF-HSCs. The numbers of TUNEL

and Annexin V positive nuclei (green) were divided by the total numbers of nuclei determined by DAPI staining (blue). At least 5 images were taken for each group. Values represent mean ± SE (** $p < 0.01$).

Figure 3

Markers of apoptosis are increased in mouse myofibroblasts derived from hepatic stellate cells (MF-HSCs) that lack Nogo-B.

MF-HSCs were treated with 1μM staurosporine (STS) for 0, 2, 4, 6, 8 and 10 hours. **A.** A representative western blot analysis of apoptotic markers, including cleaved PARP, cleaved caspase-3, -8 and -9, and Bcl-xL. β-actin was used as a loading control. **B.** Quantification of western blot analysis from at least three to five independent experiments. Values represent mean ± SE (*$p < 0.05$ and **$p < 0.01$).

Figure 4

Lack of Nogo-B does not influence hepatocyte apoptosis in response to staurosporine (STS).

Hepatocytes were isolated from wild-type (WT) and NGB KO mice and treated with 10μM STS for 0, 2, 4, 6, 8 and 10 hours. Heat shock protein 90 (Hsp90) was used as a loading control.

Figure 5

Knockdown of Nogo-B increases apoptosis in human hepatic stellate cells (LX2).

LX2 cells with or without Nogo-B siRNA were treated with 100nM staurosporine (STS) for 0, 2, 4, 6, 8 and 10 hours. Western blot analysis for apoptotic markers, including cleaved PARP, cleaved caspase-3 and -9, and Bcl-xL, was performed. β-actin was used as a loading control.

Figure 6

Overexpression of Nogo-B blocks apoptosis in human hepatic stellate cells (LX2).

LX2 cells were transfected with HA-tagged human Nogo-B plasmid to overexpress Nogo-B. Cells were treated with 100nM staurosporine (STS) for 8 hours. Representative immunofluorescence images of HA and cleaved caspase-3 in LX2 cells 8 hours after STS treatment (green: HA, red: cleaved caspase-3, blue: DAPI). Arrows indicate HA-Nogo-B positive cells. Scale bar; 20μm. Cleaved caspase-3 positive cells were counted in LX-2 cells with and without Nogo-B overexpression and divided by the total numbers of nuclei, respectively. At least 8 images were taken per group. Values represent mean $\pm$ SE (** $p < 0.01$).

Figure 7

Lack of Nogo-B increases ER stress-induced apoptosis in mouse myofibroblasts derived from hepatic stellate cells (MF-HSCs).

A. MF-HSCs were treated with tunicamycin (0, 0.5, 1, 2, 5 and 10 μg/mL) for 24 hours. A representative western blot analysis (left panel) from at least three to five independent experiments and quantification of cleaved caspase-3 and -8 levels (right panels). Bip was used as an ER stress marker and β-actin was used as a loading control. Values represent mean $\pm$ SE (**$p < 0.01$). **B.** MF-HSCs were treated with 50 ng/mL Fas ligand (FasL) for 10 hours in the presence of 20 ng/mL cycloheximide (CHX), and blotted for cleaved PARP, cleaved caspase-3 and -8, and Nogo-B. β-actin was used as a loading control. **C.** A diagram of apoptotic pathways that includes a putative role of Nogo-B. At least three major apoptotic pathways exist, including the death receptor-, mitochondria- and ER stress-mediated pathways. Nogo-B reduces MF-HSC apoptosis by protecting cells from ER stress. Bcl-xL: anti-apoptotic molecule.

References

1. Bataller R: Liver fibrosis, Journal of Clinical Investigation 2005, 115:209-218
2. Friedman SL: Mechanisms of Hepatic Fibrogenesis, Gastroenterology 2008, 134:1655-1669
3. Friedman SL: Hepatic stellate cells: protean, multifunctional, and enigmatic cells of the liver, Physiol Rev 2008, 88:125-172
4. Torok NJ: Recent advances in the pathogenesis and diagnosis of liver fibrosis, J Gastroenterol 2008, 43:315-321
5. Saile B, Knittel T, Matthes N, Schott P, Ramadori G: CD95/CD95L-mediated apoptosis of the hepatic stellate cell. A mechanism terminating uncontrolled hepatic stellate cell proliferation during hepatic tissue repair, Am J Pathol 1997, 151:1265-1272
6. Cariers A, Reinehr R, Fischer R, Warskulat U, Haussinger D: c-Jun-N-terminal kinase dependent membrane targeting of CD95 in rat hepatic stellate cells, Cell Physiol Biochem 2002, 12:179-186
7. Gong W, Pecci A, Roth S, Lahme B, Beato M, Gressner AM: Transformation-dependent susceptibility of rat hepatic stellate cells to apoptosis induced by soluble Fas ligand, Hepatology 1998, 28:492-502
8. Novo E: Overexpression of Bcl-2 by activated human hepatic stellate cells: resistance to apoptosis as a mechanism of progressive hepatic fibrogenesis in humans, Gut 2005, 55:1174-1182
9. Taimr P: Activated stellate cells express the TRAIL receptor-2/death receptor-5 and undergo TRAIL-mediated apoptosis, Hepatology 2003, 37:87-95
10. Abriss B: Adenoviral-mediated transfer of p53 or retinoblastoma protein blocks cell proliferation and induces apoptosis in culture-activated hepatic stellate cells, Journal of Hepatology 2003, 38:169-178
11. Aziz SA, Longxi P, Buwu F, Yuan W, Sinan G: Expression of p53 in the Effects of Artesunate on

Induction of Apoptosis and Inhibition of Proliferation in Rat Primary Hepatic Stellate Cells, PLoS ONE 2011, 6:e26500

12. Lim MP, Devi LA, Rozenfeld R: Cannabidiol causes activated hepatic stellate cell death through a mechanism of endoplasmic reticulum stress-induced apoptosis, Cell Death and Disease 2011, 2:e170

13. Wang X, Ikejima K, Kon K, Arai K, Aoyama T, Okumura K, Abe W, Sato N, Watanabe S: Ursolic acid ameliorates hepatic fibrosis in the rat by specific induction of apoptosis in hepatic stellate cells, Journal of Hepatology 2011, 55:379-387

14. Iredale JP: Cirrhosis: new research provides a basis for rational and targeted treatments, BMJ 2003, 327:143-147

15. Bataller R, Brenner DA: Hepatic stellate cells as a target for the treatment of liver fibrosis, Semin Liver Dis 2001, 21:437-451

16. Elsharkawy AM, Oakley F, Mann DA: The role and regulation of hepatic stellate cell apoptosis in reversal of liver fibrosis, Apoptosis 2005, 10:927-939

17. Teng FY, Tang BL: Cell autonomous function of Nogo and reticulons: The emerging story at the endoplasmic reticulum, J Cell Physiol 2008, 216:303-308

18. Oertle T, Schwab ME: Nogo and its paRTNers, Trends Cell Biol 2003, 13:187-194

19. Chen MS, Huber AB, van der Haar ME, Frank M, Schnell L, Spillmann AA, Christ F, Schwab ME: Nogo-A is a myelin-associated neurite outgrowth inhibitor and an antigen for monoclonal antibody IN-1, Nature 2000, 403:434-439

20. GrandPre T, Nakamura F, Vartanian T, Strittmatter SM: Identification of the Nogo inhibitor of axon regeneration as a Reticulon protein, Nature 2000, 403:439-444

21. Prinjha R, Moore SE, Vinson M, Blake S, Morrow R, Christie G, Michalovich D, Simmons DL, Walsh

FS: Inhibitor of neurite outgrowth in humans, Nature 2000, 403:383-384

22. Huber AB, Weinmann O, Brosamle C, Oertle T, Schwab ME: Patterns of Nogo mRNA and protein expression in the developing and adult rat and after CNS lesions, J Neurosci 2002, 22:3553-3567

23. Hunt D, Coffin RS, Prinjha RK, Campbell G, Anderson PN: Nogo-A expression in the intact and injured nervous system, Mol Cell Neurosci 2003, 24:1083-1102

24. Tozaki H, Kawasaki T, Takagi Y, Hirata T: Expression of Nogo protein by growing axons in the developing nervous system, Brain Res Mol Brain Res 2002, 104:111-119

25. Yu J, Fernandez-Hernando C, Suarez Y, Schleicher M, Hao Z, Wright PL, DiLorenzo A, Kyriakides TR, Sessa WC: Reticulon 4B (Nogo-B) is necessary for macrophage infiltration and tissue repair, Proc Natl Acad Sci U S A 2009, 106:17511-17516

26. Acevedo L, Yu J, Erdjument-Bromage H, Miao RQ, Kim JE, Fulton D, Tempst P, Strittmatter SM, Sessa WC: A new role for Nogo as a regulator of vascular remodeling, Nat Med 2004, 10:382-388

27. Wright PL, Yu J, Di YP, Homer RJ, Chupp G, Elias JA, Cohn L, Sessa WC: Epithelial reticulon 4B (Nogo-B) is an endogenous regulator of Th2-driven lung inflammation, J Exp Med 2010, 207:2595-2607

28. Sutendra G, Dromparis P, Wright P, Bonnet S, Haromy A, Hao Z, McMurtry MS, Michalak M, Vance JE, Sessa WC, Michelakis ED: The role of Nogo and the mitochondria-endoplasmic reticulum unit in pulmonary hypertension, Sci Transl Med 2011, 3:88ra55

29. Marin EP, Moeckel G, Al-Lamki R, Bradley J, Yan Q, Wang T, Wright PL, Yu J, Sessa WC: Identification and regulation of reticulon 4B (Nogo-B) in renal tubular epithelial cells, Am J Pathol 2010, 177:2765-2773

30. Zhang D, Utsumi T, Huang HC, Gao L, Sangwung P, Chung C, Shibao K, Okamoto K, Yamaguchi K,

Groszmann RJ, Jozsef L, Hao Z, Sessa WC, Iwakiri Y: Reticulon 4B (Nogo-B) is a novel regulator of hepatic fibrosis, Hepatology 2011, 53:1306-1315

31. Kim JE, Li S, GrandPre T, Qiu D, Strittmatter SM: Axon regeneration in young adult mice lacking Nogo-A/B, Neuron 2003, 38:187-199

32. Zheng B, Ho C, Li S, Keirstead H, Steward O, Tessier-Lavigne M: Lack of enhanced spinal regeneration in Nogo-deficient mice, Neuron 2003, 38:213-224

33. Loureiro-Silva MR, Cadelina GW, Iwakiri Y, Groszmann RJ: A liver-specific nitric oxide donor improves the intra-hepatic vascular response to both portal blood flow increase and methoxamine in cirrhotic rats, J Hepatol 2003, 39:940-946

34. Loureiro-Silva MR, Iwakiri Y, Abraldes JG, Haq O, Groszmann RJ: Increased phosphodiesterase-5 expression is involved in the decreased vasodilator response to nitric oxide in cirrhotic rat livers, J Hepatol 2006, 44:886-893

35. Friedman SL, Roll FJ: Isolation and culture of hepatic lipocytes, Kupffer cells, and sinusoidal endothelial cells by density gradient centrifugation with Stractan, Anal Biochem 1987, 161:207-218

36. Kruglov EA, Correa PR, Arora G, Yu J, Nathanson MH, Dranoff JA: Molecular basis for calcium signaling in hepatic stellate cells, Am J Physiol Gastrointest Liver Physiol 2007, 292:G975-982

37. Passino MA, Adams RA, Sikorski SL, Akassoglou K: Regulation of hepatic stellate cell differentiation by the neurotrophin receptor p75NTR, Science 2007, 315:1853-1856

38. Wang W, Soroka CJ, Mennone A, Rahner C, Harry K, Pypaert M, Boyer JL: Radixin is required to maintain apical canalicular membrane structure and function in rat hepatocytes, Gastroenterology 2006, 131:878-884

39. Xu L, Hui AY, Albanis E, Arthur MJ, O'Byrne SM, Blaner WS, Mukherjee P, Friedman SL, Eng FJ:

Human hepatic stellate cell lines, LX-1 and LX-2: new tools for analysis of hepatic fibrosis, Gut 2005, 54:142-151

40. Laleman W, Van Landeghem L, Severi T, Vander Elst I, Zeegers M, Bisschops R, Van Pelt J, Roskams T, Cassiman D, Fevery J, Nevens F: Both Ca2+ -dependent and -independent pathways are involved in rat hepatic stellate cell contraction and intrahepatic hyperresponsiveness to methoxamine, Am J Physiol Gastrointest Liver Physiol 2007, 292:G556-564

41. Wang XM, Yu DM, McCaughan GW, Gorrell MD: Fibroblast activation protein increases apoptosis, cell adhesion, and migration by the LX-2 human stellate cell line, Hepatology 2005, 42:935-945

42. Hernandez-Munoz I, de la Torre P, Sanchez-Alcazar JA, Garcia I, Santiago E, Munoz-Yague MT, Solis-Herruzo JA: Tumor necrosis factor alpha inhibits collagen alpha 1(I) gene expression in rat hepatic stellate cells through a G protein, Gastroenterology 1997, 113:625-640

43. Hu Y, Benedict MA, Wu D, Inohara N, Nunez G: Bcl-XL interacts with Apaf-1 and inhibits Apaf-1-dependent caspase-9 activation, Proc Natl Acad Sci U S A 1998, 95:4386-4391

44. Adams JM, Cory S: The Bcl-2 protein family: arbiters of cell survival, Science 1998, 281:1322-1326

45. Iredale JP, Benyon RC, Pickering J, McCullen M, Northrop M, Pawley S, Hovell C, Arthur MJ: Mechanisms of spontaneous resolution of rat liver fibrosis. Hepatic stellate cell apoptosis and reduced hepatic expression of metalloproteinase inhibitors, J Clin Invest 1998, 102:538-549

46. Wright MC, Issa R, Smart DE, Trim N, Murray GI, Primrose JN, Arthur MJP, Iredale JP, Mann DA: Gliotoxin Stimulates the Apoptosis of Human and Rat Hepatic Stellate Cells and Enhances the Resolution of Liver Fibrosis in Rats, Gastroenterology 2001, 121:685-698

47. Kisseleva T, Cong M, Paik Y, Scholten D, Jiang C, Benner C, Iwaisako K, Moore-Morris T, Scott B, Tsukamoto H, Evans SM, Dillmann W, Glass CK, Brenner DA: Myofibroblasts revert to an inactive

phenotype during regression of liver fibrosis, Proc Natl Acad Sci U S A 2012, 109:9448-9453

48. Paik YH, Kim JK, Lee JI, Kang SH, Kim DY, An SH, Lee SJ, Lee DK, Han KH, Chon CY, Lee SI, Lee KS, Brenner DA: Celecoxib induces hepatic stellate cell apoptosis through inhibition of Akt activation and suppresses hepatic fibrosis in rats, Gut 2009, 58:1517-1527

49. Lee JI, Lee KS, Paik YH, Nyun Park Y, Han KH, Chon CY, Moon YM: Apoptosis of hepatic stellate cells in carbon tetrachloride induced acute liver injury of the rat: analysis of isolated hepatic stellate cells, J Hepatol 2003, 39:960-966

50. Voeltz GK, Prinz WA, Shibata Y, Rist JM, Rapoport TA: A class of membrane proteins shaping the tubular endoplasmic reticulum, Cell 2006, 124:573-586

51. Jimbo A, Fujita E, Kouroku Y, Ohnishi J, Inohara N, Kuida K, Sakamaki K, Yonehara S, Momoi T: ER stress induces caspase-8 activation, stimulating cytochrome c release and caspase-9 activation, Exp Cell Res 2003, 283:156-166

52. Green DR: Apoptotic pathways: the roads to ruin, Cell 1998, 94:695-698

53. Ashkenazi A, Dixit VM: Apoptosis control by death and decoy receptors, Curr Opin Cell Biol 1999, 11:255-260

54. Ashkenazi A, Dixit VM: Death receptors: signaling and modulation, Science 1998, 281:1305-1308

55. Tagami S, Eguchi Y, Kinoshita M, Takeda M, Tsujimoto Y: A novel protein, RTN-XS, interacts with both Bcl-XL and Bcl-2 on endoplasmic reticulum and reduces their anti-apoptotic activity, Oncogene 2000, 19:5736-5746

56. Li Q, Qi B, Oka K, Shimakage M, Yoshioka N, Inoue H, Hakura A, Kodama K, Stanbridge EJ, Yutsudo M: Link of a new type of apoptosis-inducing gene ASY/Nogo-B to human cancer, Oncogene 2001, 20:3929-3936

57. Oertle T, Merkler D, Schwab ME: Do cancer cells die because of Nogo-B?, Oncogene 2003, 22:1390-1399

58. Canbay A, Friedman S, Gores GJ: Apoptosis: the nexus of liver injury and fibrosis, Hepatology 2004, 39:273-278

Figure 1

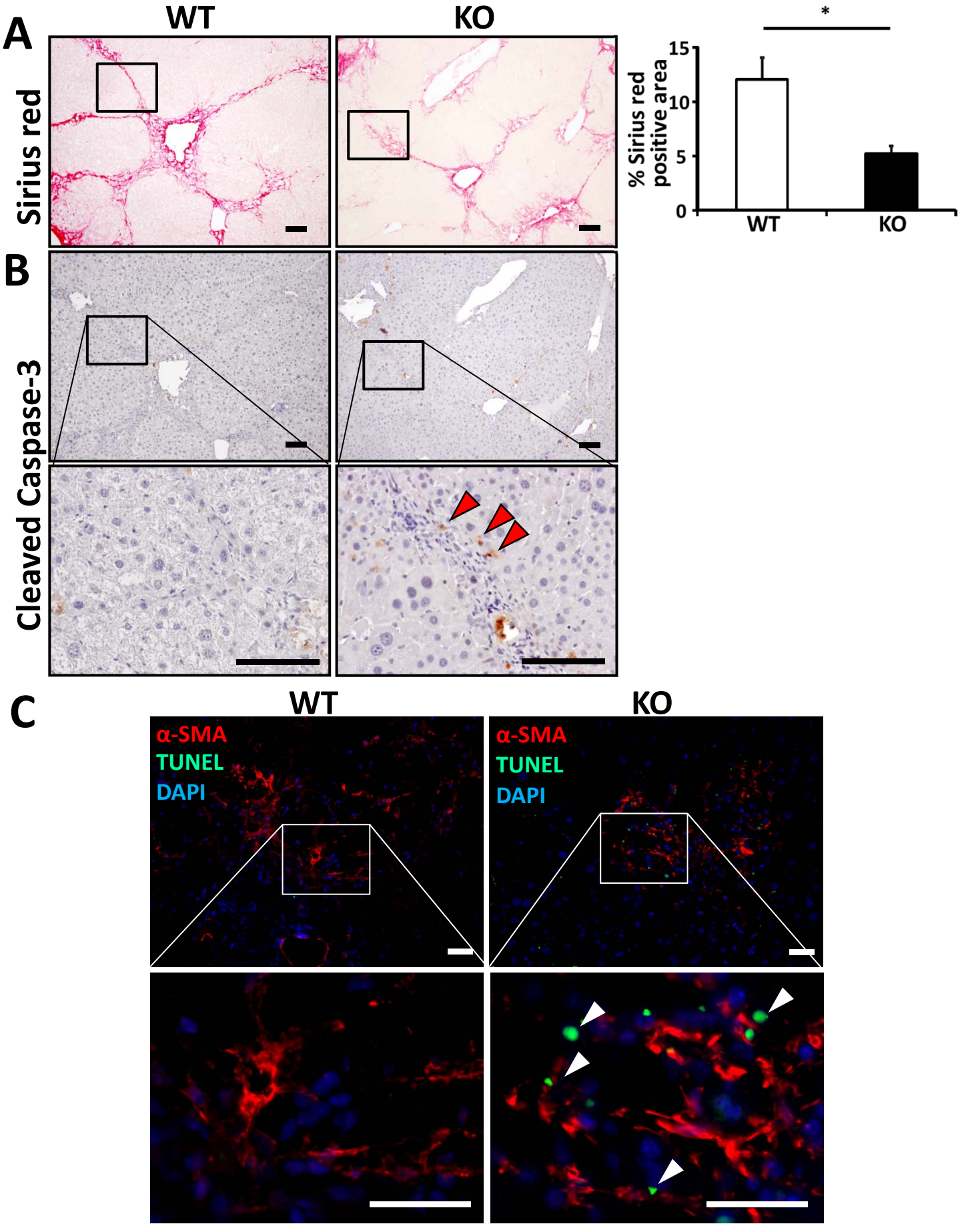
A
WT
KO
Sirius red
*
% Sirius red positive area
15
10
5
0
WT
KO
B
Cleaved Caspase-3
C
WT
KO
α-SMA
TUNEL
DAPI
α-SMA
TUNEL
DAPI

Figure 7

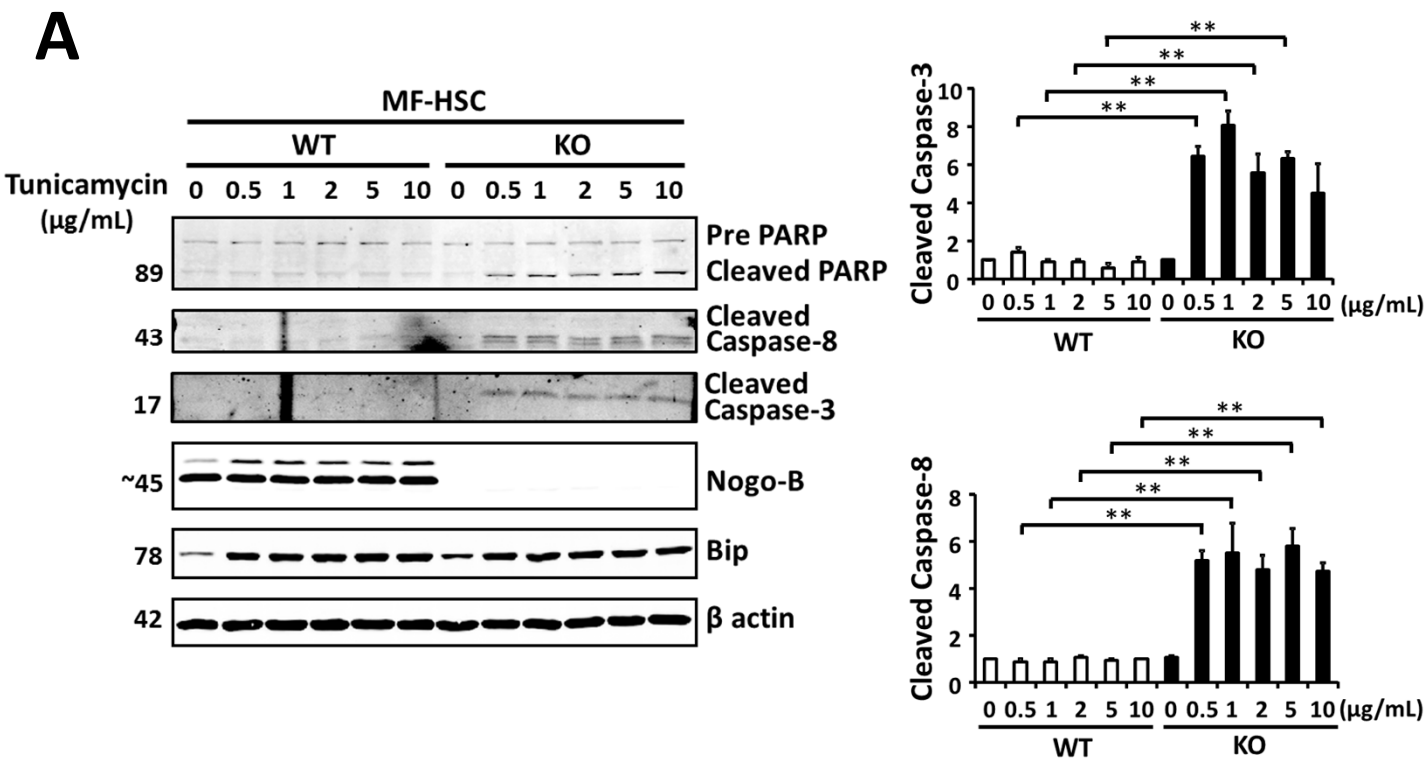
A
MF-HSC
WT
KO
Tunicamycin (μg/mL)
0 0.5 1 2 5 10 0 0.5 1 2 5 10
89
Pre PARP
Cleaved PARP
43
Cleaved Caspase-8
17
Cleaved Caspase-3
~45
Nogo-B
78
Bip
42
β actin
Cleaved Caspase-3
Cleaved Caspase-8
**
0 0.5 1 2 5 10 0 0.5 1 2 5 10 (μg/mL)
WT
KO

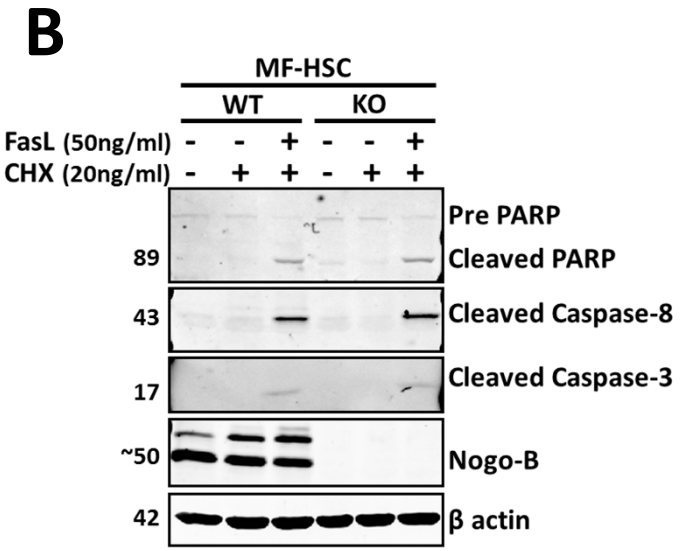
B
MF-HSC
WT
KO
FasL (50ng/ml) - - + - - +
CHX (20ng/ml) - + + - + +
89
Pre PARP
Cleaved PARP
43
Cleaved Caspase-8
17
Cleaved Caspase-3
~50
Nogo-B
42
β actin

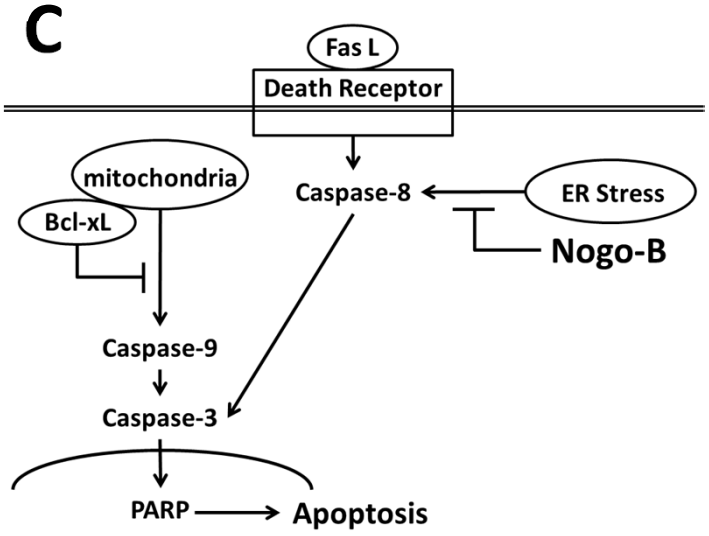
C
Fas L
Death Receptor
mitochondria
Bcl-xL
Caspase-8
ER Stress
Nogo-B
Caspase-9
Caspase-3
PARP
Apoptosis

Figure 2

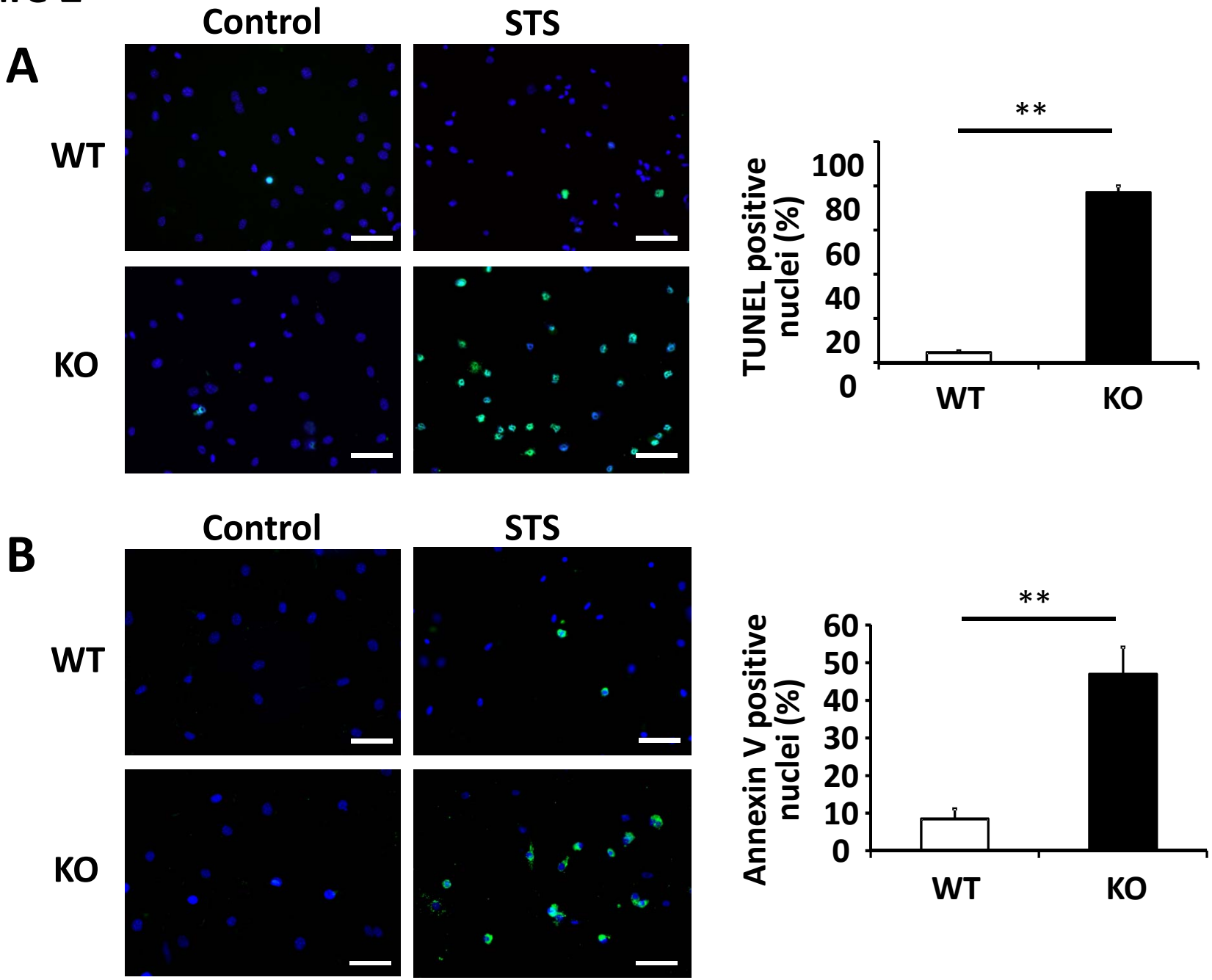
A
Control
STS
WT
KO
TUNEL positive nuclei (%)
100
80
60
40
20
0
**
WT
KO
B
Control
STS
WT
KO
Annexin V positive nuclei (%)
60
50
40
30
20
10
0
**
WT
KO

Figure 3

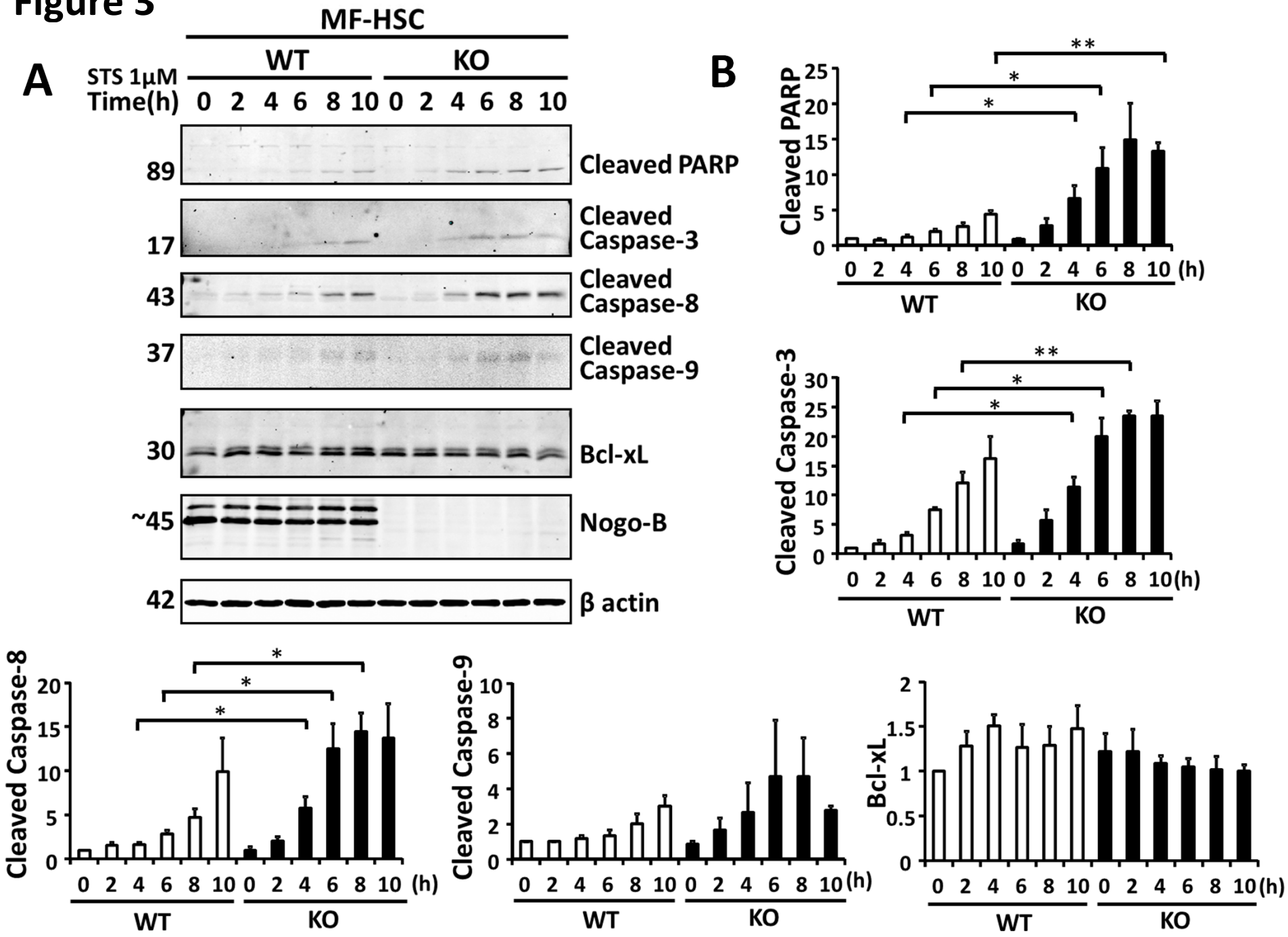
A
MF-HSC
WT
KO
STS 1μM
Time(h) 0 2 4 6 8 10 0 2 4 6 8 10
89
Cleaved PARP
17
Cleaved Caspase-3
43
Cleaved Caspase-8
37
Cleaved Caspase-9
30
Bcl-xL
~45
Nogo-B
42
β actin
B
Cleaved PARP
Cleaved Caspase-3
Cleaved Caspase-8
Cleaved Caspase-9
Bcl-xL
0 2 4 6 8 10 0 2 4 6 8 10 (h)
WT
KO
*
**

Figure 4

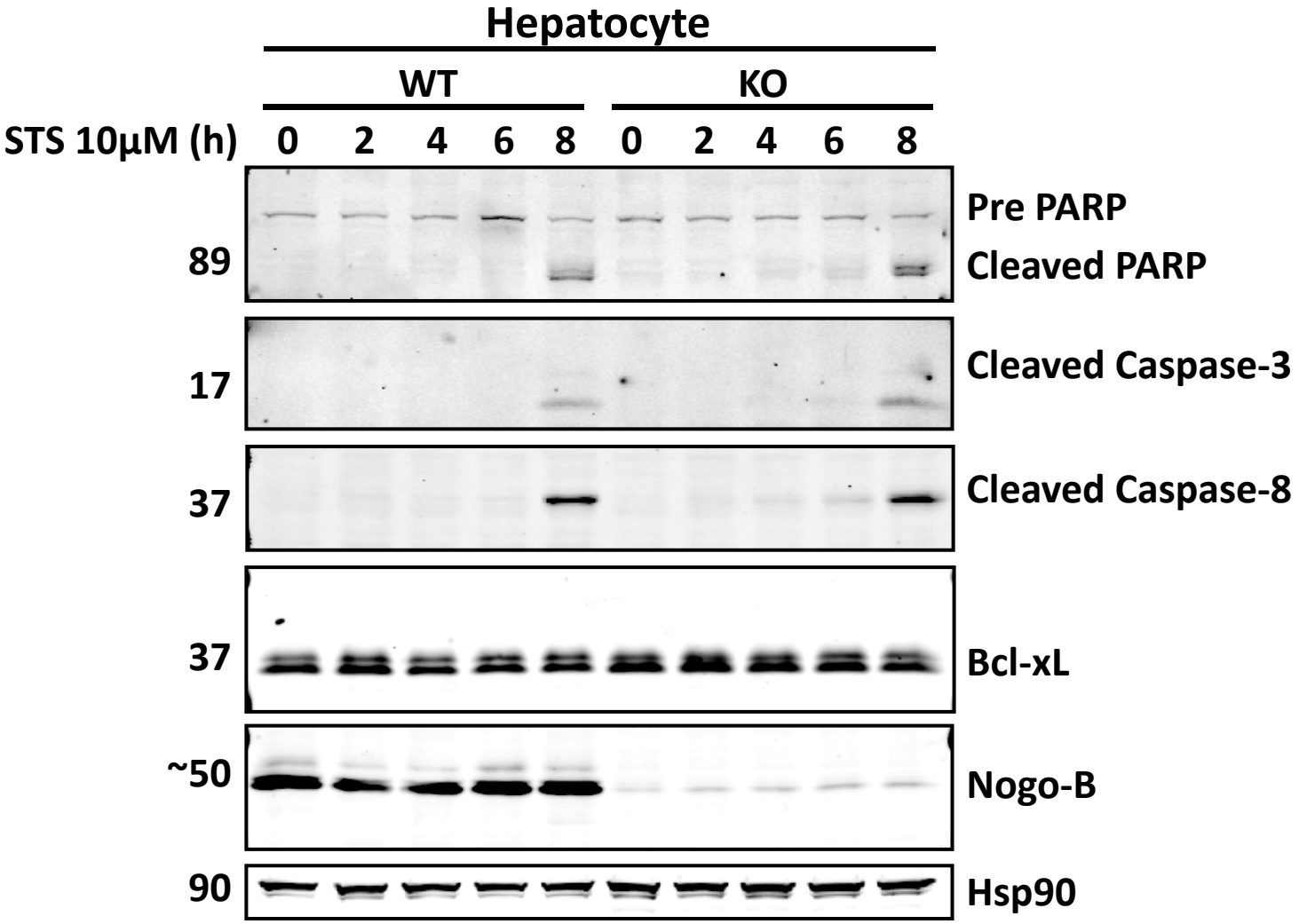
Hepatocyte
WT
KO
STS 10μM (h)
0 2 4 6 8 0 2 4 6 8
89
Pre PARP
Cleaved PARP
17
Cleaved Caspase-3
37
Cleaved Caspase-8
37
Bcl-xL
~50
Nogo-B
90
Hsp90

Figure 5

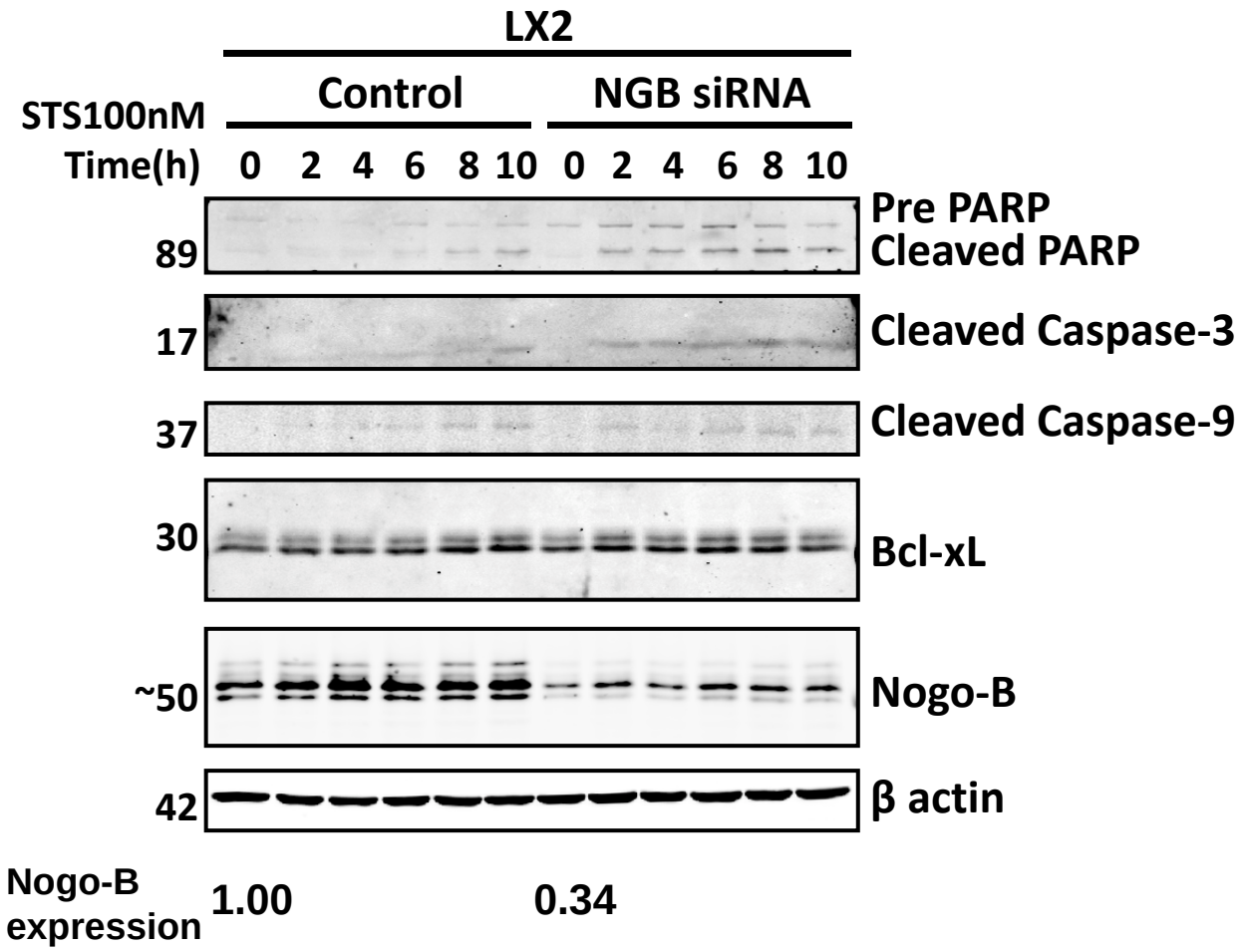
LX2
STS100nM
Control
NGB siRNA
Time(h)
0 2 4 6 8 10 0 2 4 6 8 10
89
Pre PARP
Cleaved PARP
17
Cleaved Caspase-3
37
Cleaved Caspase-9
30
Bcl-xL
~50
Nogo-B
42
β actin
Nogo-B expression
1.00
0.34

Figure 6

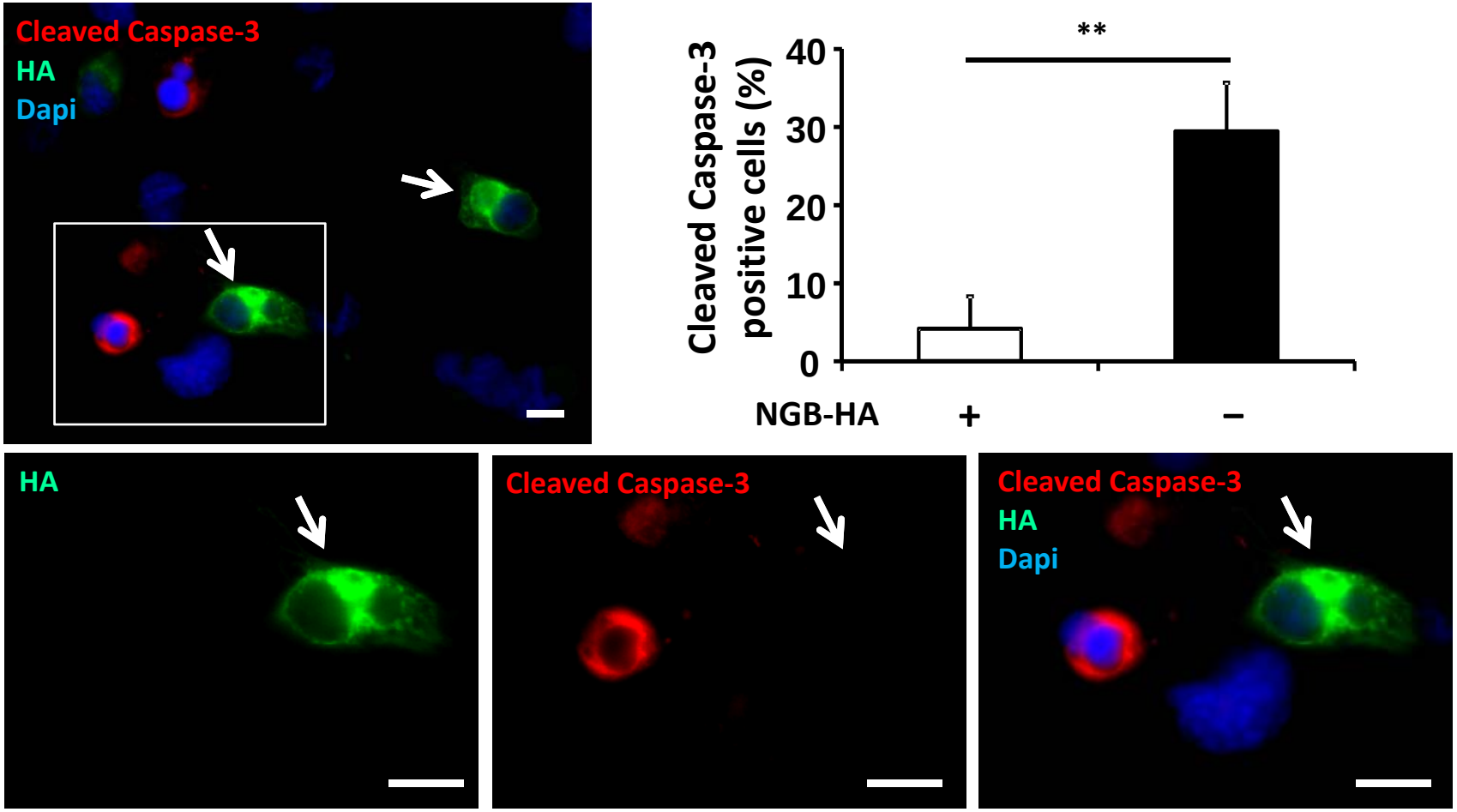
Cleaved Caspase-3
HA
Dapi
**
Cleaved Caspase-3 positive cells (%)
40
30
20
10
0
NGB-HA
+
–
HA
Cleaved Caspase-3
Cleaved Caspase-3
HA
Dapi